# Reconstruction and localization of auditory sources from intracerebral SEEG using independent component analysis

Víctor López-Madrona, Samuel Medina Villalon, Jayabal Velmurugan, Aurore Semeux-Bernier, Elodie Garnier, Jean-Michel Badier, Daniele Schön, Christian-G. Bénar

Version of Record: https://www.sciencedirect.com/science/article/pii/S1053811923000538
Manuscript_caae6ed99b512b6610438a939d4f97ab

# Reconstruction and localization of auditory sources from intracerebral SEEG using independent component analysis

Víctor J. López-Madrona[1], Samuel Medina Villalon[1,2], Jayabal Velmurugan[1], Aurore Semeux-Bernier[1], Elodie Garnier[1], Jean-Michel Badier[1], Daniele Schon[1], Christian G. Bénar[1]

1 Aix Marseille Univ, INSERM, INS, Inst Neurosci Syst, Marseille, 13005, France.
2 APHM, Timone Hospital, Epileptology and cerebral rhythmology, Marseille, 13005, France.

**ABSTRACT**

Stereo-electroencephalography (SEEG) is the surgical implantation of electrodes in the brain to better localize the epileptic network in pharmaco-resistant epileptic patients. This technique has exquisite spatial and temporal resolution. Still, the number and the position of the electrodes in the brain is limited and determined by the semiology and/or preliminary non-invasive examinations, leading to a large number of unexplored brain structures in each patient. Here, we propose a new approach to reconstruct the activity of non-sampled structures in SEEG, based on independent component analysis (ICA) and dipole source localization. We have tested this approach with an auditory stimulation dataset in ten patients. The activity directly recorded from the auditory cortex served as ground truth and was compared to the ICA applied on all non-auditory electrodes. Our results show that the activity from the auditory cortex can be reconstructed at the single trial level from contacts as far as ~40 mm from the source. Importantly, this reconstructed activity is localized via dipole fitting in the proximity of the original source. In addition, we show that the size of the confidence interval of the dipole fitting is a good indicator of the reliability of the result, which depends on the geometry of the SEEG implantation. Overall, our approach allows reconstructing the activity of structures far from the electrode locations, partially overcoming the spatial sampling limitation of intracerebral recordings.

**KEY WORDS:** source reconstruction, intracerebral recordings, independent component analysis, inverse problem, dipole fitting

## INTRODUCTION

Intracerebral recordings in the form of stereo-electroencephalography (SEEG; Bancaud et al., 1970) represent one of the most accurate approaches to measure brain activity, with a high temporal and spatial resolution. However, SEEG implantation is restricted to presurgical evaluation of epilepsy (but see Scullen et al., 2021), and the electrode locations are determined by clinical aspects, strongly constraining the number of accessible areas. Inverse modelling has been extensively applied to EEG and magnetoencephalography (MEG) data to reconstruct and localize sources that are generated far from sensors (Baillet et al., 2001; Grech et al., 2008). A few studies have attempted to transfer these methodologies to SEEG (Cam et al., 2017; Caune et al., 2014; Chang et al., 2005; Hosseini et al., 2018; Satzer et al., 2022; Yvert et al., 2005), opening the possibility to record the activity from structures not sampled with intracerebral electrodes. Most of them are based on simulations (Cam et al., 2017; Caune et al., 2014; Chang et al., 2005; Hosseini et al., 2018; Yvert et al., 2005) or intracerebral electrical stimulation (Caune et al., 2014) and require further testing on physiological activity. In Cam et al., 2017 and Caune et al., 2014, they also tested their approach to localize the source of epileptic spikes in a single patient, but it required a prior identification of the spikes from the ground truth.

There are two main goals when solving the inverse problem: the localization of the sources and the reconstruction of their time-course. Equivalent current dipoles and distributed source solutions aim at explaining the activation map or topography recorded at the contact level, with different mathematical constraints (Cam et al., 2017; Caune et al., 2014; Satzer et al., 2022; Yvert et al., 2005). A complementary approach in inverse modelling are spatial filters (or “beamforming”; Sekihara et al., 2001). This method computes a spatial filter independently for each source location, reconstructing the activity at the desired point instead of obtaining the best location for a certain topography. It allows constructing virtual electrodes in non-sampled structures, increasing the spatial coverage of SEEG. To our knowledge, only two studies have attempted to reconstruct the time course of the sources in SEEG, but they were limited to simulations (Cam et al., 2017; Chang et al., 2005).

Independent component analysis (ICA) is a popular technique in EEG and MEG that aims to separate the activities of different sources mixed at the contact level. It has been widely used to remove artifacts (Jung et al., 2000) and to retrieve the time-courses of neuronal sources (Sohrabpour et al., 2020), both in pathology (Malinowska et al., 2014; Pizzo et al., 2019) and cognition (Hsu et al., 2022; López-Madrona et al., 2022; Tang et al., 2005). It allows the segregation of the specific time-courses associated to either artefactual or physiological generators, which improves the signal-to-noise ratio (Ding et al., 2007; Lemm et al., 2006; Yang et al., 2011) and may also retrieve activities hidden in the raw data (López-Madrona et al., 2022). Moreover, the spatial profile of the components (i.e., the mixing matrix with the contribution of the components to each contact) can be used to estimate the origin of the source (Delorme et al., 2012). Although intracerebral electrodes are placed in structures of interest and are assumed to record the local activity, they are not immune to the volume conduction from other areas. Studies in animals have proven the utility of ICA to disentangle local and remote activities (Herreras et al., 2015; López-Madrona et al., 2020; Torres et al., 2019), and it is starting to be applied on human studies to re-referencing the data (Michelmann et al., 2018), remove the electrical reference (Hu et al., 2007; Whitmore and Lin, 2016) or to separate multiple hippocampal sources (Lopez-Madrona et al., 2022). Indeed, ICA offers a solution to retrieve the time-courses of colocalized neuronal generators, otherwise impossible with classic montages (Herreras et al., 2022).

In this work, we propose to use ICA on SEEG to both reconstruct the time-course of sources far from the recording sites and to localize them precisely within the brain. This work is structured as follows: first, we have recorded the auditory evoked potentials (AEPs) from epileptic patients with an electrode passing through auditory regions during the presentation of binaural pure tones. We used this activity as the ground truth. Then, we studied the capacity of ICA to retrieve the auditory activity from contacts located far from the auditory cortex (Heschl's gyrus and Planum Temporale). Finally, we applied source localization on the spatial profiles of the independent components to estimate their origin within the brain.

## METHODS

### Participants

Ten patients (6 females) with pharmacoresistant epilepsy were recorded with SEEG during their period of presurgical evaluation. Table 1 shows the clinical information for each patient. All the patients presented, one electrode passing through the Heschl's gyrus and the Planum Temporale, targeting the thalamus (electrode H; Figure 1a), and at least three other electrodes surrounding the auditory cortex. Participants were selected based on this criterion and they do not belong to a consecutive series of experiments. Recording the Heschl's gyrus and Planum Temporale is critically important because of its connections with lower central regions and the inferior frontal gyrus: it is a pathway through which seizures from the temporal pole and the anterior superior temporal gyrus generalize. Neuropsychological assessment carried out before SEEG recordings indicated that all patients had intact language functions and met the criteria for normal hearing. None of them had their epileptogenic zone within the auditory areas as identified by experienced epileptologists. This research has been approved by the relevant Institutional Review Board (Comité de Protection des Personnes Sud-Méditerranée I, ID-RCB 2012-A00644–39). All participants signed a written informed consent form regarding this research.

| ***Patient*** | **Date acquisition** | **Age** | **Gender** | **Language organization** | **Analyzed hemisphere** |
|---|---|---|---|---|---|
| *1* | 2018 | 44 | M | Typical | Left |
| *2* | 2019 | 20 | F | Typical | Right |
| *3* | 2019 | 37 | F | Typical | Left |
| *4* | 2015 | 25 | M | Typical | Left |
| *5* | 2018 | 48 | F | Typical | Left |
| *6* | 2018 | 37 | F | Typical | Left |
| *7* | 2015 | 33 | M | Typical | Right |
| *8* | 2018 | 37 | F | Atypical | Right |

| | | | | | |
|---|---|---|---|---|---|
| *9* | 2017 | 35 | F | Typical | Left |
| *10* | 2018 | 56 | F | Typical | Right |

**Table 1: Clinical information of each patient.**

### Image acquisition

An MRI was recorded for each patient as part as the clinical routine with a 1.5 T system (Siemens, Erlangen, Germany). The MRI protocol included, among other, a T1-weighted gradient-echo and a 3D-gradient echo T1 sequence after gadolinium-based contrast agents (GBCA) injection. One day after SEEG implantation, a CT scan was performed by Optima CT 660 (General Electric Healthcare, 120 kV, 230–270 FOV, 512 × 512 matrix, 0.6 mm slice thickness). To determine the exact location of each electrode and contact, we used GARDEL (Medina Villalon et al., 2018). This tool performs the co-registration of the pre-implantation MRI to the post-implantation CT scan and the semi-automatic electrodes localization and labelling. Briefly, GARDEL co-registers the MRI to the CT image, using SPM toolbox with normalized mutual information as cost function.

### SEEG recordings

Intracerebral SEEG recordings were performed using depth electrodes, implanted in stereotactic conditions (Talairach et al., 1992; Alcis, Besançon, France, and Dixi Medical, Chaudefontaine, France). For each patient, we focused only on one hemisphere that included an electrode located in the auditory cortex (Heschl's gyrus and Planum Temporale). Electrodes implanted in the contralateral hemisphere were not included in the analysis. Each patient had between 12 and 18 electrodes implanted. The electrodes had between 8 and 15 contacts, with a diameter of 0.8 mm, 2 mm contact length and separated from each other by 1.5 mm. We acquired between 126 and 200 SEEG contacts per patient from the analyzed hemisphere (total contacts recorded: 1639; mean of 164 contacts per patient, standard deviation (s.d.) ± 23). A scalp electrode placed at Fz was used as reference for the recordings. SEEG signal was recorded on a digital system (Natus Medical Incorporated) with sampling at 1024 Hz or more with 16-bit

resolution, a hardware high-pass filter (cutoff = 0.16 Hz), and an antialiasing low-pass filter (cutoff = 340 Hz or more, depending on the sampling rate).

It is important here to clarify that there is no "standard" electrode implantation. Implantation strategy depends only on the hypotheses made about the anatomical location of the epileptogenic zone (EZ), with the aim of defining subsequent cortectomy. One of the most frequent regions to be explored is the perisylvian region in order to know for instance if the patient's epilepsy is temporal, temporo-perisylvian, or perisylvian (the main cause of surgical failure in temporal epilepsy is a misdiagnosis of perisylvian epilepsies). Perisylvian epilepsy can be localized in insular cortex, frontal opercular, parietal opercular, temporal opercular cortices and superior temporal and supramarginal gyri. In this region, electrodes are implanted orthogonally to the cortical surface in order to record along one single electrode both posterior insula, tip of Heschl's gyrus and planum temporale, for example. The transverse gyrus (Heschl's gyrus, which includes the auditory cortex) is critically important because of its connections with lower central regions and the inferior frontal gyrus: it is a pathway through which seizures from the temporal pole and the anterior superior temporal gyrus generalize.

**Experimental stimuli**

The auditory stimuli consisted in 100 pure tone trials, 30 ms long, presented binaurally at 1 kHz. The interval between stimuli was 1.030 (±200) ms. We selected this type of stimulus due to its efficiency to functionally activate and thus to map the auditory cortex (Liégeois-Chauvel et al., 1994). Patients were in a sound-attenuated room while passively listening to the pure tones from loudspeakers. Stimuli were presented using E-prime 1.1 (Psychology Software Tools Inc., Pittsburgh, PA, USA).

**Independent component analysis**

ICA is a blind source separation method that aims at solving the ‘cocktail party’ problem by separating $N$ statistically independent sources that have been mixed on $M$ recording contacts (where $N \leq M$). To identify the sources, ICA assumes that they are immobile in space, i.e., that their proportional contributions to the contacts do not change during the recording

session. Each recorded signal $u_m(t)$ is thus modeled as the sum of $N$ independent sources ($s_n(t)$) multiplied by a mixing matrix ($V_{mn}$):

$$u_m(t) = \sum_{n=1}^{N} V_{mn} s_n(t) \, , m = 1,2, \dots , M \quad (1)$$

where $u_m(t)$ is the SEEG data, $V_{mn}$ the ICA weights or spatial profiles of the sources, $M$ the number of contacts, $N$ the number of sources and $s_n(t)$ the obtained independent components ("IC-SEEGs").

We applied ICA at two different levels: on the electrode located in the auditory areas, to retrieve the specific time-course of the local neural sources (i.e., the ground truth), and on all the other contacts (without the electrode in the auditory areas) to reconstruct the same activity from purely volume conducted fields (Makarov et al., 2010). In both cases, ICA was applied on the continuous data and was set for obtaining as many components as available contacts ($N = M$; Artoni et al., 2018). ICA was computed with the Fieldtrip Matlab (Mathworks, Natick MA) toolbox (Oostenveld et al., 2011). We used the infomax algorithm, which aims to minimize the mutual information between components (Bell and Sejnowski, 1995), and was implemented originally in EEGLAB (Delorme and Makeig, 2004).

**Identification of local auditory activity with ICA**

To obtain the time-course of the auditory source - used as ground truth - we applied ICA only on the electrode in the auditory cortex (Figure 1, a-d). For each patient, we kept only the components representing a putative local source, i.e., those with a sharp spatial profile (peaking at one contact and with an abrupt decay in the adjacent channels rather than a progressive decrease; Figure 1c), and we computed the AEP (Figure 1d). There are many auditory sources that underly AEPs (Liégeois-Chauvel et al., 1994, 1991), and we identified between 2 and 4 components with a significant AEP per patient (2.6 ± 0.8 components per patient, mean ± s.d.). To test the significance of the response, we applied a t-test to check whether the activity was different from zero across trials, obtaining a *t*- and *p*-value for each time-point. The t-values were then corrected for multiple comparisons using a local false discovery rate (LFDR; Benjamini and Heller, 2007) with a threshold of 0.2. We considered that a component had an AEP if its

response was significant during at least 20 ms. For simplicity, we only chose the component with the highest response in amplitude in order to test the present approach. We labeled this component as IC-Aud, and we determined its position as the contact contributing the most to the ICA (H8 in Figure 1c). More details about the localization of auditory sources in intracranial recordings can be found in (Yvert et al., 2005). We decided to use ICA to identify the ground truth in order to facilitate its comparison with the reconstructed source, minimizing the contribution from other non-related sources (for example the reference contact, or volume conducted activities).

**Reconstruction of remote activity with ICA**

To retrieve the auditory source from remote contacts, i.e., the component identified in the auditory cortex (IC-Aud), we applied ICA on the continuous data (concatenating all the trials) of all the contacts except the electrode in the auditory cortex (Figure 1e). We computed the zero-lag Pearson correlation coefficient between the obtained components and IC-Aud (i.e., ground truth) and selected only the component with the highest correlation value (Figure 2f). We considered it as the putative auditory source, representing the activity from the auditory cortex, but recorded by remote contacts (IC-remAud). The correlation coefficient was used as an indicator of the quality of the temporal reconstruction.

We explored how the contact location affected the reconstruction of the source by computing multiple ICAs. To do so, we created a sphere around the source and progressively increased its radius (Figure 1e). First, we considered all the contacts within the sphere for ICA analysis. We started from the closest contact to the source, and we included, at each iteration, the next closest contact into the analysis (Figure 2a). We computed for each patient as many ICAs as available contacts, selecting only the component with the highest correlation with IC-Aud. To analyze the trend of the correlation values with distance, we identified the distance for highest correlation and used this point to split the data in two sections for distances smaller or higher. A linear model was fitted for each section and patient, obtaining the associated trend or β value. We excluded the value with highest correlation from the analysis, so it did not contribute to the trend. Then, we tested whether the β values of the sections before (or after) the maximum were significantly different from zero across patients with a t-test. A positive or

negative trend would suggest that for higher distances (i.e., increasing the number of contacts in the analysis), the time-course reconstruction improves or decreases, respectively.

We repeated a similar analysis but selecting the contacts outside the volume, i.e., removing the closest contact at each iteration. Starting with all electrodes (excluding the electrode in the auditory cortex), we removed the closest contact at each iteration, computing a new ICA (Figure 3a). Finally, we measured the correlation coefficient between the continuous time-courses of the reconstructed source (IC-remAud) and the ground truth (IC-Aud).

**Detection of trend changepoints**

The visual inspection of the ICA results for individual patients when removing the closest contact at a time revealed the presence of a changepoint that modified the general trend of the data (Figure 3b; Sharma et al., 2016). To better characterize this changepoint, we applied the Matlab (Mathworks, Natick, MA) function *findchangepts*. This function identifies the points where the mean and the slope of the signal change most abruptly (Haynes et al., 2017). Thus, it detects at which distance the accuracy of the identification of the auditory activity decays, which can be used as an estimation of the maximal distance from the source for a successful time-course reconstruction. We further corroborated the presence of a changepoint by testing the improvement of the linear fit if the data was divided into two sections (before and after the changepoint) or if all points were included in a single regression. However, splitting the data overfits the model and always decreases the residuals. For each patient, we computed the Bayesian Information Criterion (BIC) on the residuals of both cases (one versus two sections) to penalize the subdivision of the data. Then, we tested whether the BIC was significantly lower when the data was split in two sections with a paired t-test across patients.

**Simulation of auditory sources**

To analyze whether ICA can localize auditory sources in a controlled scenario, we simulated a dipole in the Heschl's gyrus of each patient and used ICA to localize it using the contacts far from the auditory cortex. For each patient, we selected the Heschl's gyrus (Anterior transverse temporal gyrus) using the Destrieux atlas (Destrieux et al., 2010) and located a dipole at the center of gravity of the cortical patch, with a transverse orientation to the cortex. We

computed a forward model on the cortex surface using the OpenMEEG (Gramfort et al., 2010) Boundary Element Method (BEM) method from Brainstorm (Destrieux et al., 2010). Conductivity values of 1, 0.0333 and 1 S/m were considered for the scalp, the skull and the brain, respectively. We simulated the AEP using a Gaussian pulse of 8 Hertz. This potential was projected 100 times (i.e., 100 trials) to all the sensors of each patient using the gain matrix at the dipole location. We tuned the signal-to-noise ratio to be equivalent to that observed during the task. We identified the contact with the highest AEP in amplitude during the pure tone task located in the auditory cortex and scaled the gain matrix so the Gaussian pulse had the same amplitude as the AEP. Then, we used real activity from the contacts as noise, measuring their activity during resting state. Thus, the activity of each contact was composed by resting activity plus the projected pulse.

**Identification of putative auditory sources**

We followed the approach for source localization in both the simulated and the real data. We changed our selection criterion of the putative auditory source to approximate a real-life situation where the activity of the real source is unknown. We selected a volume around the expected location (i.e., the electrode at the Heschl's gyrus) with a radius of 40 mm, and computed ICA using the electrodes within the volume. The electrode in the auditory cortex was not included in this analysis. We analyzed the AEP of all IC-SEEG to determine which one was related to the auditory activity. We selected only those components with a significant response (see "Identification of local auditory activity with ICA"). IC-remAud was determined as the IC-SEEG with highest AEP in amplitude. In 2 out of 10 patients, there were no significant AEPs among all the obtained IC-SEEGs. Due to the difficulty of identifying the auditory source with a sufficient degree of confidence in these cases, we excluded them from further source localization analysis.

**Source localization of independent components**

To localize the sources identified with ICA, we solved the inverse problem using the ICA spatial profiles (Figure 1g). First, each subject's MRI was segmented using FreeSurfer (http://surfer.nmr.mgh.harvard.edu/) and realigned in Brainstorm (Tadel et al., 2011) using six

fiducials (nasion, left and right tragus, anterior and posterior commissure, and an interhemispheric point). This yields a semi-realistic single shell volume conduction model (Nolte, 2003). All the MRI volume was considered as source space, using the OpenMEEG BEM for the forward model. Note that this forward model is not the same as the one used for the simulated source, which was computed on the cortex surface. Conductivity values of 1, 0.0333 and 1 S/m were considered for the scalp, the skull and the brain, respectively. We generated an isotropic grid with a resolution of 3.5 mm, where each grid point was associated to a triplet of orthogonal dipoles. Finally, we computed the sources using the dipole modeling from Brainstorm. A dipole scan was then applied to the ICA spatial profile, obtaining a goodness of fit (GOF) value for each grid point (Delorme et al., 2012; López-Madrona et al., 2022). We repeated the dipole scan with a more classical approach, selecting the amplitude of the AEP at the peak of the response. The peak was defined as the time with maximal amplitude when averaging the AEPs across contacts.

**Comparison of electrode anatomical configuration**

To test the influence of the electrode position on source localization, we compared two anatomical configurations on the same patients: with three electrodes either surrounding the auditory cortex (*Around* configuration) or on one side of the source (*Side*; Figure 4c). We selected three electrodes in both cases to have a comparable number of contacts in all cases. For each configuration, we identified the remote auditory source (IC-remAud). Then, we use dipole fitting to localize the source, defining a confidence interval (CI) as all the grid points with a GOF higher than 0.9 times the maximum GOF. For the analysis of Figure 4b, we also considered factors of 0.95 and 0.80 for the CI, yielding equivalent results (not shown). We tested whether both configurations yielded different results in terms of time-course reconstruction and localization. For source reconstruction, we used a paired Wilcoxon test comparing the correlation values between IC-Aud and IC-remAud in *Around* versus *Side* configurations. To test the reliability of source localization we compared if the GOF, the distance from the dipole to the source and the size of the CI were different between *Around* and *Side* (paired Wilcoxon test).

**Data and code availability statement**

The conditions of our ethics approval do not permit public archiving of anonymized study data. Readers seeking access to the data should contact the lead author. Access will be granted to named individuals in accordance with ethical procedures governing the reuse of clinical data, including completion of a formal data sharing agreement.

All the code necessary to produce the results here were performed in MATLAB software, using FieldTrip Toolbox (http://www.fieldtriptoolbox.org, Oostenveld et al., 2011), Brainstorm (https://neuroimage.usc.edu/brainstorm/, Tadel et al., 2011) and Anywave (https://meg.univ-amu.fr/wiki/AnyWave, Colombet et al., 2015), and are available upon request.

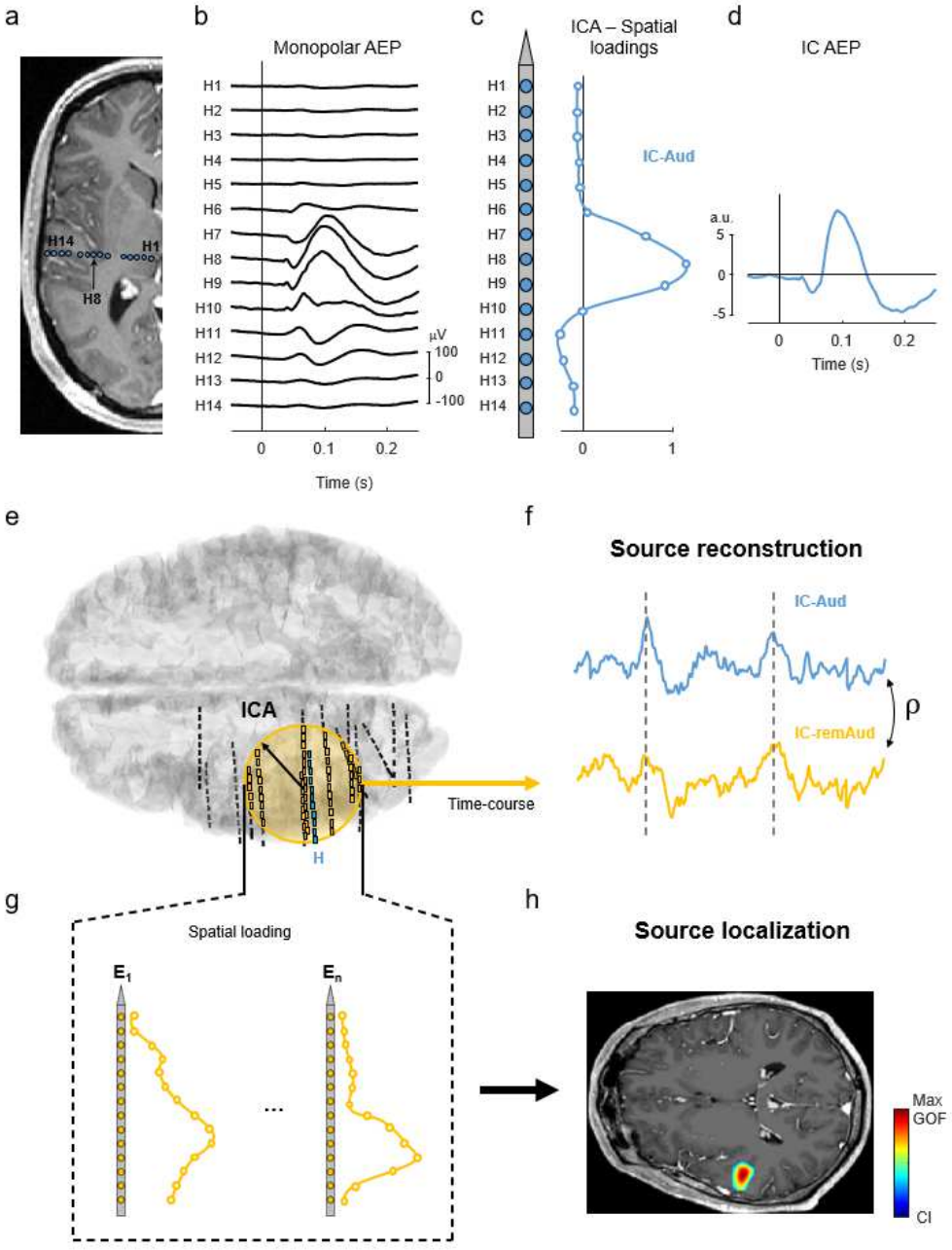


**Figure 1: Overview of the pipeline for data analysis.**

a) MRI (3D T1) with reconstruction of SEEG "H" electrode for one patient, targeting auditory cortical areas. The location of each recording site is represented with blue points.
b) Averaged AEP for pure tones at each recording site (monopolar reference).
c) Spatial profile of the IC-Aud across the electrode, representing the contribution of the independent component to each contact. The source is possibly located at (or very close to) the contact with the highest contribution (here H8).
d) Averaged AEP of the auditory component (IC-Aud).

e) Reconstruction of SEEG implantation in one patient. Dashed lines are the electrodes, where each cylinder corresponds to one contact. The yellow sphere illustrates the volume around the auditory cortex that was considered in the analysis and the arrow represent the radius of the sphere. ICA was applied on all contacts within the sphere (yellow lines). The blue line depicts the H electrode, not included in the ICA.
f) The continuous time-courses obtained with ICA on the nearby contacts are then compared with the "ground truth" (IC-Aud) using correlation. We selected the component with highest correlation (IC-remAud) as representing the activity spread by volume conduction from the auditory cortex. Dashed lines represent the peak of two responses to the pure tone stimulation.
g) Example of the spatial loadings of IC-remAud across two of the electrodes included in the analysis. The activity is well distributed across contacts and electrodes, indicating its remote origin. The gradient of the topography can be used to infer the location of the source, with higher values when the source is close.
h) Single dipole source localization of IC-remAud using the spatial profile of the ICA (panel g). Colored area represents the confidence interval.

## RESULTS

### Reconstruction of auditory signals from remote contacts

We investigated whether the activity of auditory cortex can be obtained from contacts that are in the surrounding structures to reconstruct the same time-course. For each patient, we computed as many ICAs as available contacts, increasing, progressively, the radius of the sphere around the source (Figure 1e), including all the contacts within the volume but excluding the electrode in the auditory cortex. In Figure 2a we plotted the correlation values between IC-Aud and IC-remAud for all the patients and iterations. The best results were obtained for distances of 33 mm in average (Figure 2c), with an associated correlation value of 0.38 across patients (Figure 2b). For each patient, we selected the distance that gave the highest correlation, as an estimation of the optimal volume to compute ICA. In contrast, the correlation values were considerably smaller when all the available contacts were included in the analysis (0.20 ± 0.05, mean ± s.d.). We tested the trend of the correlation values for distances closer or further than the maximum. For short distances (~33 mm), including more contacts improves the reconstruction ($p<0.01$, t-test of β values across patients higher than zero, see Methods). However, the inclusion of contacts farther than 33 mm not only does not improve the separation, but it decreases the correlation values ($p<0.001$, t-test of β values lower than zero). Note that the correlation was computed for the continuous time-courses (i.e., concatenating all trials, figure 2d). These values were much higher when considering the averaged AEP (Figures 2f and 2g). A similar increasing tendency was also identified for shorter distances (Figure 2e, $p<0.001$, t-test of β values higher than zero). However, the reconstruction of the AEP remains high, with no significant effect when adding further contacts ($p<0.48$, t-test of β values different than zero). Although we focused on only one component (IC-Aud), we also analyzed the best time-course reconstruction values for all the other components with an AEP identified in the electrode within the auditory cortex. For these components, the average correlation value across patients for the best time-course reconstruction was 0.221 ± 0.1 (mean ± s.d.) for the continuous traces and 0.87 ± 0.05 for the averaged AEP.

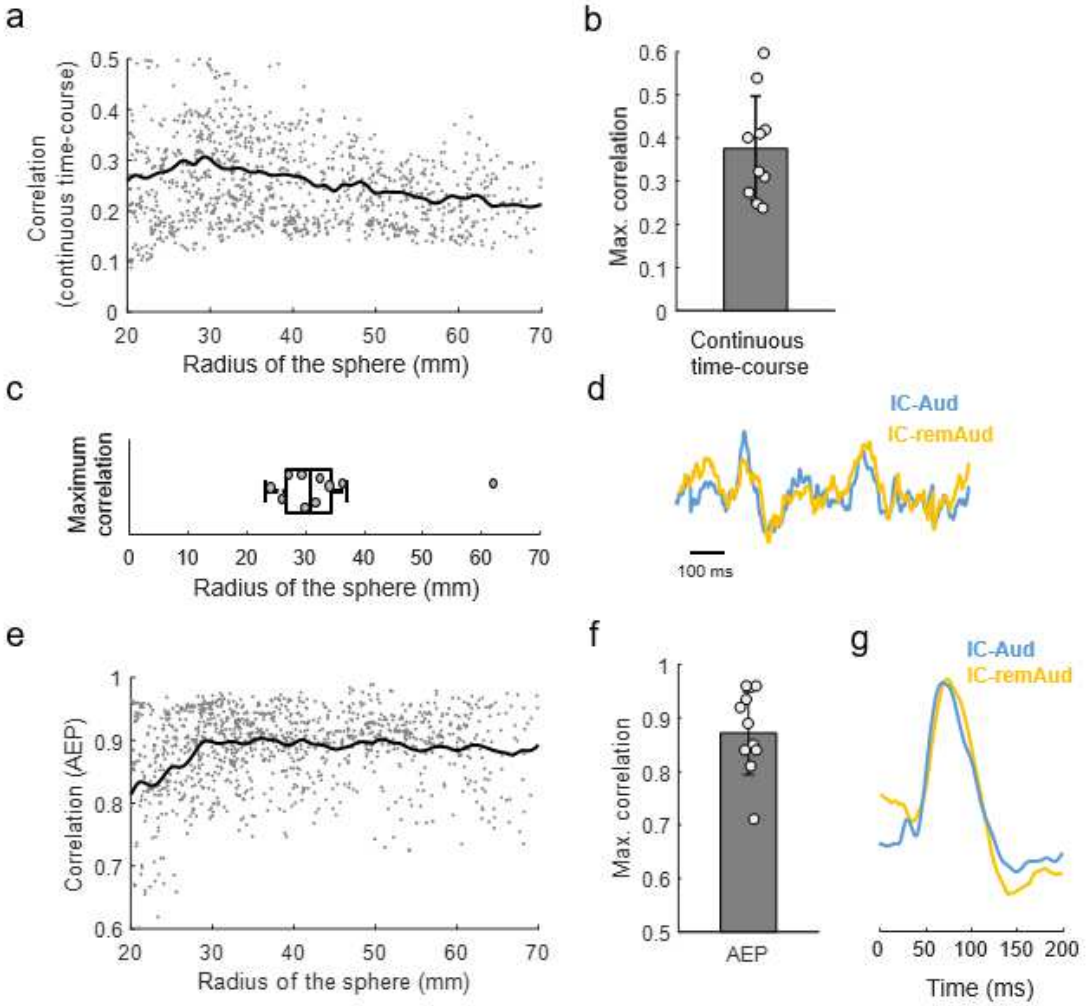


**Figure 2: Accuracy of time-course reconstruction.**

a) Correlation between the source (IC-Aud) and the most similar component obtained from afar (IC-remAud). For each radius of the sphere, only contacts within the volume were considered for ICA. Grey points represent the correlation values for each patient and radius, and the black trace is the average across points.
b) Maximum correlation values between the continuous time-courses of IC-Aud and IC-remAud for each patient (mean ± s.d. across patients).
c) For each patient, radius of the sphere that maximizes the correlation between IC-Aud and IC-remAud (panel b). For all boxplots, the central mark of the box indicates the median, and the edges of the box indicate the 25th and 75th percentiles. The whiskers extend to the most extreme data points not considered outliers. Individual values are represented as single points.
d) Example of the continuous source activity (blue) and the reconstructed signal (yellow) for patient 1. The distance from the furthest contact to the source was 43 mm and the correlation value between the whole time-courses was 0.54.
e) Same as panel a but correlating the averaged AEP instead of the continuous time-course.
f) Correlation values between AEPs of IC-Aud and IC-remAud for the radius values of panel b (mean ± s.d. across patients).
g) Example of the AEP of the source (blue) and the reconstructed AEP (yellow).

Then, we tested which distance from the source was the minimum necessary to reconstruct the auditory time-course. Similar to the previous analysis, we performed an iterative ICA increasing the radius of the sphere and selecting the component with maximum correlation. However, in this analysis we considered the contacts outside the volume (Figure 3a). As expected, the exclusion of the closest contacts decreases the correlation (closer contacts would have more information than farther ones). Interestingly, we could observe the presence of a changepoint that interrupted the general trend (green line, Figure 3b). The ICA reconstruction is relatively stable when some close contacts are included in the analysis up to that point (Figure 3b, top), with a slow decay in some cases (Figure 3b, bottom). After the changepoint, the reconstruction reaches its minimum in an approximately flat trend. We considered this threshold as the limit of the detectability of the field potential. To find the changepoint for each patient, we computed the distance at which the mean and the slope of the correlation values changed most significantly (Figure 3b, see methods). The existence of a changepoint was supported by a significant decrease of the BIC when the points are split in two sections (before and after the changepoint), instead of fitting all the data with a single linear regression ($p<0.01$, paired t-test across patients between BIC using one versus two sections). The average threshold distance across patients was 40.37 mm (Figure 3c), suggesting that electric fields generated in the auditory cortex can be captured on continuous traces up to ~40 mm from the source.

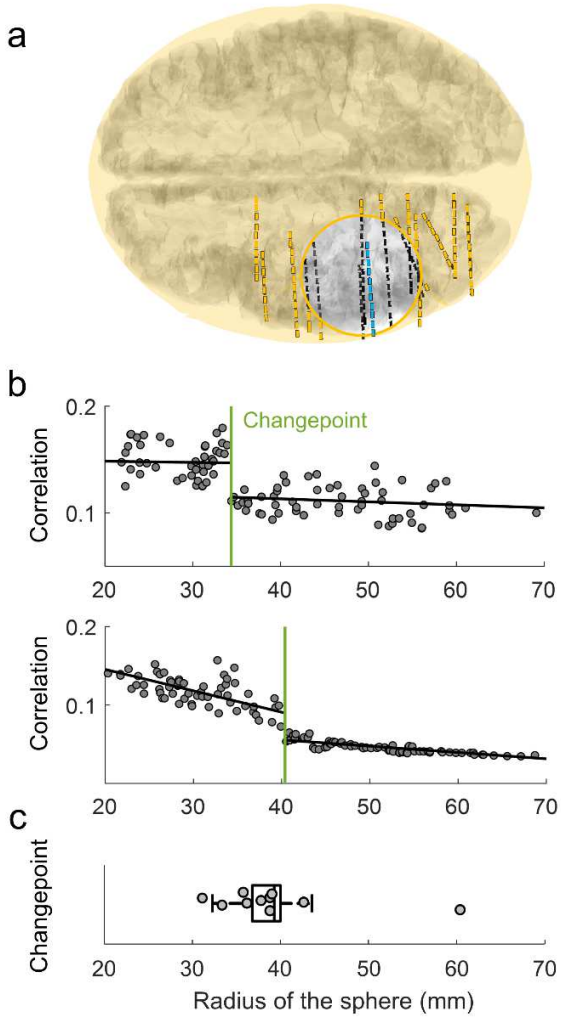


**Figure 3: Analysis of maximum distance for time-course reconstruction.**

a) Example of the electrode selection in one iteration. For a given sphere radius, only contacts outside the volume (yellow points) are considered for ICA analysis.
b) Examples of correlation between the source (IC-Aud) and the most similar component obtained from afar (IC-remAud) for patients 3 (top) and 7 (bottom). For each radius of the sphere, only contacts outside the volume were considered for ICA. Grey points represent the correlation values for each radius. Changepoint (green line) is determined as the distance with highest change in the mean and slope of the correlation values (black lines).
c) Radius of the sphere at the changepoint across patients.

## Source localization based on ICA spatial profiles

Finally, we questioned whether ICA could identify where the activity originated from. To test the effectiveness of ICA in a controlled scenario, we simulated a dipole in the Heschl's gyrus

of each patient that projected a gaussian pulse to the surrounding electrodes (see Methods). Based on the results shown in Figure 2c and Figure 3c, we fixed a volume of 40 mm radius around the source to compute ICA and identified the component with the pulse (IC-remAud). We applied a single dipole fit on the spatial distribution of IC-remAud and measured the distance from the source to the best dipole location (Figure 4a). The results presented an accurate precision in source localization, with 7 out of 8 patients showing localization errors lower than 5 mm (Figure 4b). We repeated the same analysis with an isotropic lead field (i.e., same conductivity values for the three compartments) without differences in the localization error (results not shown). If, instead of the true dipole location, the contact with highest AEP in amplitude is selected as source location (as for the real data) the localization errors were higher (11.02 ± 4.35 mm), with an average distance between the contact and the true location (i.e., simulated dipole) of 11.4 ± 2.8 mm.

We followed the same approach to localize the real AEP identified during the task (IC-Aud). For each patient, we selected the putative auditory component (IC-remAud) as the component with highest AEP, without a preselection based on the highest correlation with IC-Aud (see Methods). The average localization error was 16.87 mm, ranging from 7.8 mm to 25.65 mm (Figure 4c). We replicated the analysis but using the amplitude of the AEP at the peak instead of ICA for source localization. The localization error presented more fluctuations across patients, ranging from 8.02 mm to 47.77 mm (mean 25.59 mm). However, there were no significant differences between both modalities ($p=0.17$, paired t-test between the localization error using ICA versus the AEP).

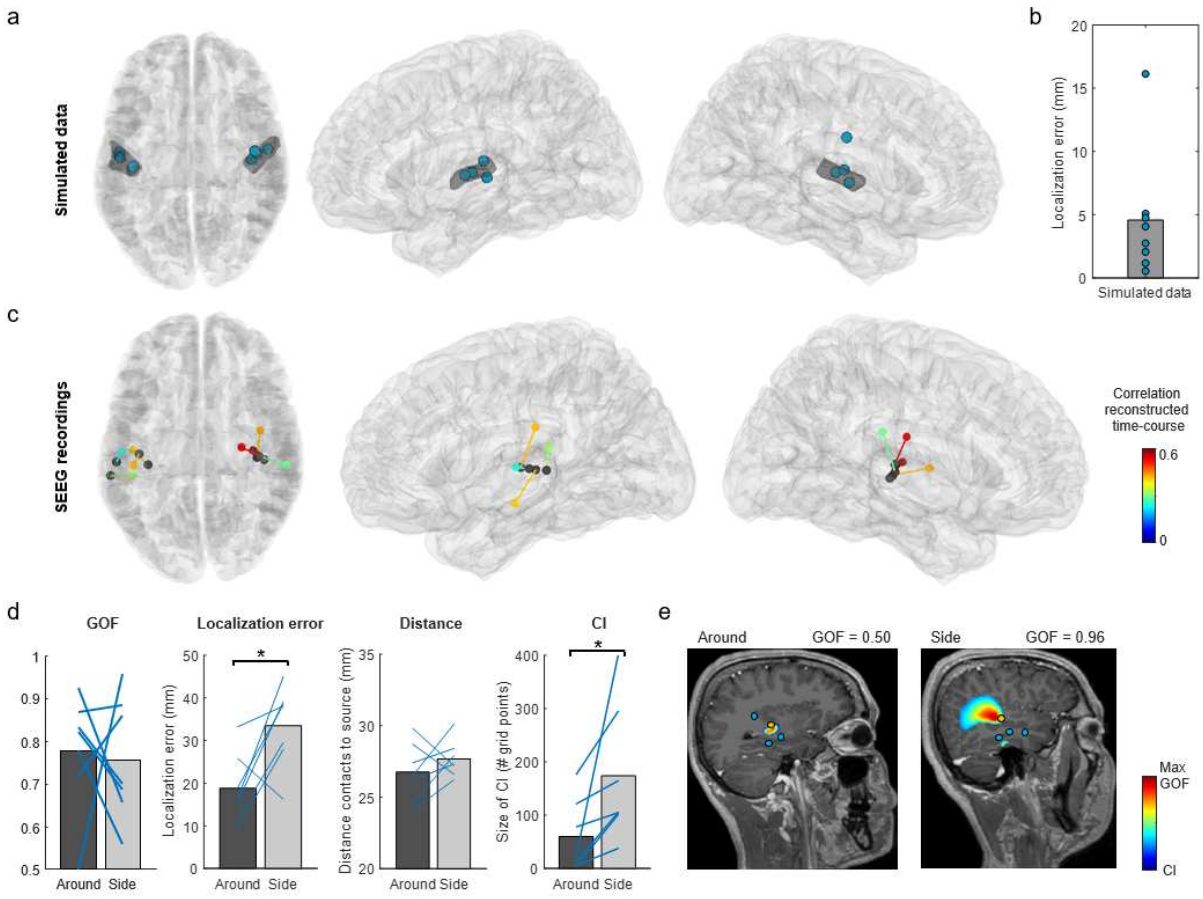


**Figure 4: Source localization of independent components**

a) Dipole localization of a simulated source in the Heschl's gyrus (shaded area). Blue dots represent the solutions for each patient.
b) Localization error from the dipole to the source for the simulated source.
c) Best dipole localization for those patients with a significant AEP. Color points represent the location of each dipole and the correlation between the time-course of the auditory source (IC-Aud) and the reconstructed signal (IC-remAud). Each dipole is linked to a grey point in the specific location of the source for that patient obtained from the electrode in the Heschl's gyrus.
d) From left to right: best goodness of fit, localization error from the dipole to the source, averaged distance from the contacts to the source and size of the CI for each patient with two different electrode configurations, either selecting three electrodes around the source (*Around*) or on one side of the source (*Side*). Blue lines link the values of each patient (*, $p<0.05$, Wilcoxon test).
e) Example of source localization for two different electrode configurations on the same patient. (Left) Three electrodes (blue points) were selected around the source (yellow point). The best localization was close to the source, with a reduced CI within the electrodes. (Right) The three electrodes were selected only on one side of the source. Although the GOF is higher in this case, the considerable size of the CI increases the uncertainty of the result and suggests that the geometry of electrode placement is not adequate for proper source localization.

In contrast with the reconstruction of the time-course, the main factor for source localization is the anatomical configuration of the electrodes. To test how the electrode positions conditioned the localization, we compared two different configurations for each patient: one with contacts surrounding the source (*Around*), and another with the electrodes covering only one side of the source (*Side;* Figure 4e). To facilitate the comparison, we used three electrodes on each patient and configuration, which were closer than 40 mm to the source (Figure 3c). One patient was excluded from this analysis as there were only three electrodes within the 40 mm radius volume (i.e., impossibility of having two different configurations). There was no difference between both configurations (*Around* and *Side*) neither in time-course reconstruction ($p=0.81$, paired Wilcoxon test between the correlation of IC-Aud and IC-remAud on each configuration, N=7) nor in GOF for the localization ($p=0.81$, paired Wilcoxon test; Figure 4d). The averaged distance from all the contacts to the source was 26.8 mm and 27.7 mm for the *Around* and *Side* configuration, respectively, without significant differences between both groups at the group level ($p=0.39$, paired Wilcoxon test; Figure 4d). However, they presented clear differences in the distance from the dipole to the location of the source ($p<0.05$, paired Wilcoxon test; Figure 4d) and the size of the CI ($p<0.05$, paired Wilcoxon test between electrode configurations, N=7; Figure 4d). If the selected contacts confined the source, the CI was narrow and between the electrodes (Figure 4e, left). However, if the source was outside the volume enclosed by the electrodes, the CI involved a much larger volume (Figure 4e, right).

## DISCUSSION

In this work, we propose a new ICA-based approach to source reconstruction from SEEG recordings, useful both for time-course estimation and for localization. We have validated it on auditory responses from 8 epileptic patients, using the activity recorded directly from the auditory cortex as a ground truth. The two main advantages of our methodology are (i) the reconstruction of the time-course of the source at the single trial level and (ii) the possibility of localizing precisely the spatial origin of the source. This complements and extends recent studies on source localization in SEEG (Cam et al., 2017; Caune et al., 2014; Chang et al., 2005; Hosseini et al., 2018; Satzer et al., 2022; Yvert et al., 2005).

We have evaluated the effect of distance from the electrodes to the source in time-course reconstruction. Contacts close to the source contain most of the volume-conducted potentials, while there is little contribution from far locations. We observed that the inclusion of the farthest contacts into the analysis deteriorated the reconstruction (Figure 2a). We interpret this as the fact that the incorporation of contacts without information of the source of interest (for example, channels mainly recording the activity from other sources) reduces its relative contribution to the total variance of the data, making the separation of all the sources more difficult for the ICA algorithm. Interestingly, this decrease in correlation with the inclusion of further contacts was not identified when analyzing the averaged AEP instead of the continuous time-course (Figure 2e). These results suggest that electrodes beyond 3-4 cm from the source (Figure 2c) contain little information from the auditory source while adding noise from other recorded sources. Computing ICA on all contacts is less efficient than considering a restricted area although it has a limited impact on the averaged AEP. We estimated that the maximal distance from the contacts to the source to perform time-course reconstruction is ~4 cm in the case of auditory areas (Figure 3c). Within this radius, there is a slow decay of the accuracy with the distance (Figure 3c). Up to that changepoint the trend varies, with a reduction in the reconstruction that reaches the minimum. While the electric field does spread further than this distance, its contribution to the recordings would be too low to be identified with ICA. Thus, it indicates the limit distance for ICA to separate the remote source from other components. Note that the maximal distance for time-course reconstruction may differ for other structures as the

generation and spread of field potentials depends on the geometry of the sources (Herreras, 2016). It may also vary as a function of the signal-to-noise ratio of a given activity, that depends on the amplitude of currents, level of synchrony and extent of activated cortex (Cosandier-Rimélé et al., 2008).

We have analyzed the best electrode position to perform source localization, preferably surrounding the source (Figure 4e). Importantly, we have found that CI of the dipole model, but not the GOF, is a good indicator of the reliability of the result (Figure 4d). If one has an a priori estimation of where the sources should be, as it is commonly the case in cognitive tasks, then it is possible to focus the analysis on the contacts nearby the region of interest and favor a good anatomical configuration of the electrodes to reconstruct the time-course. If we ignore the position of the source, for example in resting data, one can use the CI and the position of the dipole with respect to the surrounding electrodes to estimate the reliability of the result. When a triplet (at least) of electrodes is selected and the confidence interval is enclosed between the electrodes, there is a high chance that the equivalent dipole is close to the real source (Figure 4e, left). However, if the best solution is outside the volume delimited by the electrodes, the error in the localization can be high, even if the goodness of fit is higher than in the previous scenario (Figure 4e, right). In this case, it is recommended, if possible, to change the selected contacts for ICA analysis and use electrodes surrounding the putative source. If this is not possible, one should consider discarding the results.

Here, we used a protocol based on auditory stimuli in order to test the proposed methodology in a controlled setup. Nevertheless, one of the main advantages of ICA is that it does not rely on specific events like event-related potentials or epileptic spikes, compared to other approaches that localize the sources of a topographic map in a given time window (Cam et al., 2017, 2017; Satzer et al., 2022; Yvert et al., 2005). This has two main advantages. Firstly, it can be applied to coactivated sources separately, for example, disentangling the different sources responding to a given stimulus. Secondly, it can be extended to sources with non-time-locked activities. Thus, it could possibly detect the different active sources in resting or identify epileptic areas that were not covered with SEEG. As ICA assumes immobile sources, it remains to be investigated the impact of spreading activity on source separation remains to be

investigated. When the activity propagates to other areas, ICA should be able to decompose it in multiple well localized sources if the activities are not completely simultaneous (although ICA can separate highly correlated sources, Makarova et al., 2011). Moreover, it has been suggested that most EEG oscillations are better modeled by independent sections of coherent activity, rather than by traveling waves (Jung et al., 2001).

Although we considered the source activity measured from H as local (i.e., originated in the same spot as the H contacts), AEPs are generated all along the supratemporal plane (Liégeois-Chauvel et al., 1994, 1991). Thus, it is possible that the recorded source was originated in a nearby region (Yvert et al., 2005). To overcome this limitation, we simulated an auditory source, controlling its specific location. In this scenario, the results showed a high accuracy of ICA to localize auditory sources (Figure 4a and 4b). Another possibility to record local sources is with bipolar montages, which measure the local inward and outward currents at the contact level. However, they may not recover the specific time-courses of the neuronal generators (Fernández-Ruiz and Herreras, 2013; Herreras et al., 2022; Martín-Vázquez et al., 2013) as, for instance, in the case of colocalized sources with different activities (Herreras et al., 2022). This is an advantage of ICA over the classically used bipolar montage: one can still recover the close sources, but also the remote ones that spread on many channels. Then, it is possible to localize the source and to verify, thanks to a confidence interval, that the configuration was proper.

For each putative source, ICA retrieves its temporal and spatial information. The former corresponds to its time-course (i.e., source reconstruction), while the latter (spatial profile) can be used for source localization. By fitting a single dipole on the remote component (IC-remAud), we tracked the activity to the vicinity of the auditory cortex, with low localization errors both in simulations (Figure 4a) and real data (Figure 4c). Although the analysis using a more classical approach as the amplitude of the averaged AEP yielded no significant differences in localization error, the variance of the values across patients was much higher, while ICA yielded more stable results. The dipolar approach can be questioned in SEEG, as the closer to a source, the more non-dipolar the fields can be (Jerbi et al., 2004). To be noted, we investigated here a localization based on electrodes that do not directly sample the region of interest. In this case, it would be interesting to investigate distributed sources and whether one could reconstruct the actual

extent of activated cortex (Grova et al., 2006; Maksymenko et al., 2017). Conversely, the number of methods to compute source localization on ICA is limited. Most of them rely on the noise covariance matrix, which cannot be easily estimated from ICA spatial profiles. This restricts the optimization of its final solution, obtaining dipole positions less accurate than other methodologies (Cam et al., 2017; Caune et al., 2014). This warrants further developments, for example, with resampling method based on bootstrapping for estimating the level of noise in a given component (Luria et al., 2020).

In this work, we used a general three-compartment model for source localization. However, as both sources and contacts are restricted to the cerebral tissue, there is a limited effect of the scalp and skull conductivities in the final solution. Simpler one-layer models covering the area of interest may offer identical solutions with an important reduction of the computational cost. The anisotropy of the brain tissues has been shown to impact source localization in EEG and MEG (Bangera et al., 2010; Haueisen et al., 2002; Wolters et al., 2006). In (Wolters et al., 2006), authors estimated an improvement of 5% in the relative difference measure (RDM) when considering anisotropy in the white matter. Similar results were reported in (Bangera et al., 2010), where the improvement was between and 5 and 9% of the RDM when considering the best anisotropic model compared to an isotropic one. Future work will investigate the impact of tissue anisotropy on source localization.

Source localization based on ICA is thus a promising approach to overcome the limited spatial sampling of SEEG and to infer the actual time-course and location of a source. We show here that the field of view is of the order of 4 cm, and that the confidence interval of a dipolar localization can be used to verify that the anatomical location of the electrodes was adequate. Our results complement previous methodologies (Cam et al., 2017; Caune et al., 2014; Chang et al., 2005; Satzer et al., 2022; Yvert et al., 2005) and expands the applications of source reconstruction in SEEG. For example, our approach may identify non-sampled structures displaying epileptic spikes and seizures, complementing the clinical information during presurgical evaluation. Furthermore, it potentially permits to study the dynamics in cognition of healthy areas that are not targeted during SEEG exploration.

**ACKNOWLEDGMENTS**

Research supported by a FLAG ERA/HBP grant from Agence Nationale de la recherche "SCALES" ANR-17-HBPR-0005). This work was performed on a platform member of France Life Imaging network (grant ANR-11-INBS-0006), and it has received support from the French government under the Programme « Investissements d'Avenir », Initiative d'Excellence d'Aix-Marseille Université via A*Midex funding (AMX-19-IET-004), and ANR (ANR-17-EURE-0029). VJL was supported by a postdoctoral fellowship from the Institute of Language, Cognition and the Brain (ILCB, grant ANR-16-CONV-0002).

**Declaration of Competing Interest**

There are no conflicts of interest to declare by the authors.

**Credit authorship contribution statement**

**Víctor J. López-Madrona:** Conceptualization, Methodology, Software, Formal analysis, Writing – original draft, Visualization. **Samuel Medina Villalon:** Software, Data curation, Writing – review & editing. **Jayabal Velmurugan:** Methodology, Software, Writing – review & editing. **Aurore Semeux-Bernier:** Methodology, Software, Writing – review & editing. **Elodie Garnier:** Methodology, Software, Writing – review & editing. **Jean-Michel Badier:** Conceptualization, Methodology, Writing – review & editing. **Daniele Schon:** Investigation, Writing – review & editing, Funding acquisition. **Christian G. Bénar:** Conceptualization, Methodology, Writing – original draft, Supervision, Project administration.

## REFERENCES


Artoni, F., Delorme, A., Makeig, S., 2018. Applying dimension reduction to EEG data by Principal Component Analysis reduces the quality of its subsequent Independent Component decomposition. NeuroImage 175, 176–187. https://doi.org/10.1016/j.neuroimage.2018.03.016

Baillet, S., Mosher, J.C., Leahy, R.M., 2001. Electromagnetic brain mapping. IEEE Signal Process. Mag. 18, 14–30. https://doi.org/10.1109/79.962275

Bancaud, J., Angelergues, R., Bernouilli, C., Bonis, A., Bordas-Ferrer, M., Bresson, M., Buser, P., Covello, L., Morel, P., Szikla, G., Takeda, A., Talairach, J., 1970. Functional stereotaxic exploration (SEEG) of epilepsy. Electroencephalogr. Clin. Neurophysiol. 28, 85–86.

Bangera, N.B., Schomer, D.L., Dehghani, N., Ulbert, I., Cash, S., Papavasiliou, S., Eisenberg, S.R., Dale, A.M., Halgren, E., 2010. Experimental validation of the influence of white matter anisotropy on the intracranial EEG forward solution. J. Comput. Neurosci. 29, 371–387. https://doi.org/10.1007/s10827-009-0205-z

Bell, A.J., Sejnowski, T.J., 1995. An information-maximization approach to blind separation and blind deconvolution. Neural Comput. 7, 1129–1159. https://doi.org/10.1162/neco.1995.7.6.1129

Benjamini, Y., Heller, R., 2007. False Discovery Rates for Spatial Signals. J. Am. Stat. Assoc. 102, 1272–1281. https://doi.org/10.1198/016214507000000941

Cam, S.L., Ranta, R., Caune, V., Korats, G., Koessler, L., Maillard, L., Louis-Dorr, V., 2017. SEEG dipole source localization based on an empirical Bayesian approach taking into account forward model uncertainties. NeuroImage 153, 1–15. https://doi.org/10.1016/j.neuroimage.2017.03.030

Caune, V., Ranta, R., Le Cam, S., Hofmanis, J., Maillard, L., Koessler, L., Louis-Dorr, V., 2014. Evaluating dipolar source localization feasibility from intracerebral SEEG recordings. NeuroImage 98, 118–133. https://doi.org/10.1016/j.neuroimage.2014.04.058

Chang, N., Gulrajani, R., Gotman, J., 2005. Dipole localization using simulated intracerebral EEG. Clin. Neurophysiol. 116, 2707–2716. https://doi.org/10.1016/j.clinph.2005.07.002

Colombet, B., Woodman, M., Badier, J.M., Bénar, C.G., 2015. AnyWave: a cross-platform and modular software for visualizing and processing electrophysiological signals. J. Neurosci. Methods 242, 118–126. https://doi.org/10.1016/j.jneumeth.2015.01.017

Cosandier-Rimélé, D., Merlet, I., Badier, J.M., Chauvel, P., Wendling, F., 2008. The neuronal sources of EEG: modeling of simultaneous scalp and intracerebral recordings in epilepsy. NeuroImage 42, 135–146. https://doi.org/10.1016/j.neuroimage.2008.04.185

Delorme, A., Makeig, S., 2004. EEGLAB: an open-source toolbox for analysis of single-trial EEG dynamics including independent component analysis. J. Neurosci. Methods 134, 9–21. https://doi.org/10.1016/j.jneumeth.2003.10.009

Delorme, A., Palmer, J., Onton, J., Oostenveld, R., Makeig, S., 2012. Independent EEG sources are dipolar. PloS One 7, e30135. https://doi.org/10.1371/journal.pone.0030135

Destrieux, C., Fischl, B., Dale, A., Halgren, E., 2010. Automatic parcellation of human cortical gyri and sulci using standard anatomical nomenclature. NeuroImage 53, 1–15. https://doi.org/10.1016/j.neuroimage.2010.06.010

Ding, L., Worrell, G.A., Lagerlund, T.D., He, B., 2007. Ictal Source Analysis: Localization and Imaging of Causal Interactions in Humans. NeuroImage 34, 575–586. https://doi.org/10.1016/j.neuroimage.2006.09.042

Fernández-Ruiz, A., Herreras, O., 2013. Identifying the synaptic origin of ongoing neuronal oscillations through spatial discrimination of electric fields. Front. Comput. Neurosci. 7, 5. https://doi.org/10.3389/fncom.2013.00005

Gramfort, A., Papadopoulo, T., Olivi, E., Clerc, M., 2010. OpenMEEG: opensource software for quasistatic bioelectromagnetics. Biomed. Eng. Online 9, 45. https://doi.org/10.1186/1475-925X-9-45

Grech, R., Cassar, T., Muscat, J., Camilleri, K.P., Fabri, S.G., Zervakis, M., Xanthopoulos, P., Sakkalis, V., Vanrumste, B., 2008. Review on solving the inverse problem in EEG source analysis. J. NeuroEngineering Rehabil. 5, 1–33. https://doi.org/10.1186/1743-0003-5-25

Grova, C., Daunizeau, J., Lina, J.-M., Bénar, C.G., Benali, H., Gotman, J., 2006. Evaluation of EEG localization methods using realistic simulations of interictal spikes. NeuroImage 29, 734–753. https://doi.org/10.1016/j.neuroimage.2005.08.053

Haueisen, J., Tuch, D.S., Ramon, C., Schimpf, P.H., Wedeen, V.J., George, J.S., Belliveau, J.W., 2002. The Influence of Brain Tissue Anisotropy on Human EEG and MEG. NeuroImage 15, 159–166. https://doi.org/10.1006/nimg.2001.0962

Haynes, K., Fearnhead, P., Eckley, I.A., 2017. A computationally efficient nonparametric approach for changepoint detection. Stat. Comput. 27, 1293–1305. https://doi.org/10.1007/s11222-016-9687-5

Herreras, O., 2016. Local Field Potentials: Myths and Misunderstandings. Front. Neural Circuits 10. https://doi.org/10.3389/fncir.2016.00101

Herreras, O., Makarova, J., Makarov, V.A., 2015. New uses of LFPs: Pathway-specific threads obtained through spatial discrimination. Neuroscience 310, 486–503. https://doi.org/10.1016/j.neuroscience.2015.09.054

Herreras, O., Torres, D., Martín-Vázquez, G., Hernández-Recio, S., López-Madrona, V.J., Benito, N., Makarov, V.A., Makarova, J., 2022. Site-dependent shaping of field potential waveforms. Cereb. Cortex bhac297. https://doi.org/10.1093/cercor/bhac297

Hosseini, S.A.H., Sohrabpour, A., He, B., 2018. Electromagnetic source imaging using simultaneous scalp EEG and intracranial EEG: An emerging tool for interacting with pathological brain networks. Clin. Neurophysiol. Off. J. Int. Fed. Clin. Neurophysiol. 129, 168–187. https://doi.org/10.1016/j.clinph.2017.10.027

Hsu, S.-H., Lin, Y., Onton, J., Jung, T.-P., Makeig, S., 2022. Unsupervised learning of brain state dynamics during emotion imagination using high-density EEG. NeuroImage 249, 118873. https://doi.org/10.1016/j.neuroimage.2022.118873

Hu, S., Stead, M., Worrell, G.A., 2007. Automatic identification and removal of scalp reference signal for intracranial EEGs based on independent component analysis. IEEE Trans. Biomed. Eng. 54, 1560–1572. https://doi.org/10.1109/TBME.2007.892929

Jerbi, K., Baillet, S., Mosher, J.C., Nolte, G., Garnero, L., Leahy, R.M., 2004. Localization of realistic cortical activity in MEG using current multipoles. NeuroImage 22, 779–793. https://doi.org/10.1016/j.neuroimage.2004.02.010

Jung, T.P., Makeig, S., Humphries, C., Lee, T.W., McKeown, M.J., Iragui, V., Sejnowski, T.J., 2000. Removing electroencephalographic artifacts by blind source separation. Psychophysiology 37, 163–178.

Jung, T.-P., Makeig, S., McKeown, M.J., Bell, A.J., Lee, T.-W., Sejnowski, T.J., 2001. Imaging Brain Dynamics Using Independent Component Analysis. Proc. IEEE Inst. Electr. Electron. Eng. 89, 1107–1122. https://doi.org/10.1109/5.939827

Lemm, S., Curio, G., Hlushchuk, Y., Müller, K.-R., 2006. Enhancing the signal-to-noise ratio of ICA-based extracted ERPs. IEEE Trans. Biomed. Eng. 53, 601–607. https://doi.org/10.1109/TBME.2006.870258

Liégeois-Chauvel, C., Musolino, A., Badier, J.M., Marquis, P., Chauvel, P., 1994. Evoked potentials recorded from the auditory cortex in man: evaluation and topography of the middle latency components. Electroencephalogr. Clin. Neurophysiol. Potentials Sect. 92, 204–214. https://doi.org/10.1016/0168-5597(94)90064-7

Liégeois-Chauvel, C., Musolino, A., Chauvel, P., 1991. Localization of the primary auditory area in man. Brain J. Neurol. 114 ( Pt 1A), 139–151.

López-Madrona, V.J., Medina Villalon, S., Badier, J.-M., Trébuchon, A., Jayabal, V., Bartolomei, F., Carron, R., Barborica, A., Vulliémoz, S., Alario, F.-X., Bénar, C.G., 2022. Magnetoencephalography can reveal deep brain network activities linked to memory processes. Hum. Brain Mapp. https://doi.org/10.1002/hbm.25987

López-Madrona, V.J., Pérez-Montoyo, E., Álvarez-Salvado, E., Moratal, D., Herreras, O., Pereda, E., Mirasso, C.R., Canals, S., 2020. Different theta frameworks coexist in the rat hippocampus and are coordinated during memory-guided and novelty tasks. eLife 9. https://doi.org/10.7554/eLife.57313

Lopez-Madrona, V.J., Trebuchon, A., Mindruta, I., Barbeau, E.J., Barborica, A., Pistol, C., Oane, I., Alario, F.-X., Benar, C.G., 2022. Independent component analysis reveals an early hippocampal recognition system using intracerebral evoked potentials in humans. https://doi.org/10.1101/2022.11.02.513525

Luria, G., Duran, D., Visani, E., Rossi Sebastiano, D., Sorrentino, A., Tassi, L., Granvillano, A., Franceschetti, S., Panzica, F., 2020. Towards the Automatic Localization of the Irritative Zone Through Magnetic Source Imaging. Brain Topogr. 33, 651–663. https://doi.org/10.1007/s10548-020-00789-y

Makarov, V.A., Makarova, J., Herreras, O., 2010. Disentanglement of local field potential sources by independent component analysis. J. Comput. Neurosci. 29, 445–457. https://doi.org/10.1007/s10827-009-0206-y

Makarova, J., Ibarz, J.M., Makarov, V.A., Benito, N., Herreras, O., 2011. Parallel readout of pathway-specific inputs to laminated brain structures. Front. Syst. Neurosci. 5, 77. https://doi.org/10.3389/fnsys.2011.00077

Maksymenko, K., Giusiano, B., Roehri, N., Bénar, C.-G., Badier, J.-M., 2017. Strategies for statistical thresholding of source localization maps in magnetoencephalography and estimating source extent. J. Neurosci. Methods 290, 95–104. https://doi.org/10.1016/j.jneumeth.2017.07.015

Malinowska, U., Badier, J.-M., Gavaret, M., Bartolomei, F., Chauvel, P., Bénar, C.-G., 2014. Interictal networks in magnetoencephalography. Hum. Brain Mapp. 35, 2789–2805. https://doi.org/10.1002/hbm.22367

Martín-Vázquez, G., Makarova, J., Makarov, V.A., Herreras, O., 2013. Determining the true polarity and amplitude of synaptic currents underlying gamma oscillations of local field potentials. PloS One 8, e75499. https://doi.org/10.1371/journal.pone.0075499

Medina Villalon, S., Paz, R., Roehri, N., Lagarde, S., Pizzo, F., Colombet, B., Bartolomei, F., Carron, R., Bénar, C.-G., 2018. EpiTools, A software suite for presurgical brain mapping in epilepsy: Intracerebral EEG. J. Neurosci. Methods 303, 7–15. https://doi.org/10.1016/j.jneumeth.2018.03.018

Michelmann, S., Treder, M.S., Griffiths, B., Kerrén, C., Roux, F., Wimber, M., Rollings, D., Sawlani, V., Chelvarajah, R., Gollwitzer, S., Kreiselmeyer, G., Hamer, H., Bowman, H., Staresina, B., Hanslmayr, S., 2018. Data-driven re-referencing of intracranial EEG based on independent component analysis (ICA). J. Neurosci. Methods 307, 125–137. https://doi.org/10.1016/j.jneumeth.2018.06.021

Nolte, G., 2003. The magnetic lead field theorem in the quasi-static approximation and its use for magnetoencephalography forward calculation in realistic volume conductors. Phys. Med. Biol. 48, 3637–3652. https://doi.org/10.1088/0031-9155/48/22/002

Oostenveld, R., Fries, P., Maris, E., Schoffelen, J.-M., 2011. FieldTrip: Open source software for advanced analysis of MEG, EEG, and invasive electrophysiological data. Comput. Intell. Neurosci. 2011, 156869. https://doi.org/10.1155/2011/156869

Pizzo, F., Roehri, N., Medina Villalon, S., Trébuchon, A., Chen, S., Lagarde, S., Carron, R., Gavaret, M., Giusiano, B., McGonigal, A., Bartolomei, F., Badier, J.M., Bénar, C.G., 2019. Deep brain activities

can be detected with magnetoencephalography. Nat. Commun. 10, 971. https://doi.org/10.1038/s41467-019-08665-5
Satzer, D., Esengul, Y.T., Warnke, P.C., Issa, N.P., Nordli, D.R., 2022. SEEG in 3D: Interictal Source Localization From Intracerebral Recordings. Front. Neurol. 13, 782880. https://doi.org/10.3389/fneur.2022.782880
Scullen, T., Teja, N., Song, S.H., Couldwell, M., Carr, C., Mathkour, M., Lee, D.J., Tubbs, R.S., Dallapiazza, R.F., 2021. Use of Stereoelectroencephalography Beyond Epilepsy: A Systematic Review. World Neurosurg. 155, 96–108. https://doi.org/10.1016/j.wneu.2021.06.105
Sekihara, K., Nagarajan, S.S., Poeppel, D., Marantz, A., Miyashita, Y., 2001. Reconstructing spatio-temporal activities of neural sources using an MEG vector beamformer technique. IEEE Trans. Biomed. Eng. 48, 760–771. https://doi.org/10.1109/10.930901
Sharma, S., Swayne, D.A., Obimbo, C., 2016. Trend analysis and change point techniques: a survey. Energy Ecol. Environ. 1, 123–130. https://doi.org/10.1007/s40974-016-0011-1
Sohrabpour, A., Cai, Z., Ye, S., Brinkmann, B., Worrell, G., He, B., 2020. Noninvasive electromagnetic source imaging of spatiotemporally distributed epileptogenic brain sources. Nat. Commun. 11, 1946. https://doi.org/10.1038/s41467-020-15781-0
Tadel, F., Baillet, S., Mosher, J.C., Pantazis, D., Leahy, R.M., 2011. Brainstorm: a user-friendly application for MEG/EEG analysis. Comput. Intell. Neurosci. 2011, 879716. https://doi.org/10.1155/2011/879716
Talairach, J., Tournoux, P., Musolino, A., Missir, O., 1992. Stereotaxic exploration in frontal epilepsy. Adv. Neurol. 57, 651–688.
Tang, A.C., Sutherland, M.T., McKinney, C.J., 2005. Validation of SOBI components from high-density EEG. NeuroImage 25, 539–553. https://doi.org/10.1016/j.neuroimage.2004.11.027
Torres, D., Makarova, J., Ortuño, T., Benito, N., Makarov, V.A., Herreras, O., 2019. Local and Volume-Conducted Contributions to Cortical Field Potentials. Cereb. Cortex N. Y. N 1991 29, 5234–5254. https://doi.org/10.1093/cercor/bhz061
Whitmore, N.W., Lin, S.-C., 2016. Unmasking local activity within local field potentials (LFPs) by removing distal electrical signals using independent component analysis. NeuroImage 132, 79–92. https://doi.org/10.1016/j.neuroimage.2016.02.032
Wolters, C.H., Anwander, A., Tricoche, X., Weinstein, D., Koch, M.A., MacLeod, R.S., 2006. Influence of tissue conductivity anisotropy on EEG/MEG field and return current computation in a realistic head model: a simulation and visualization study using high-resolution finite element modeling. NeuroImage 30, 813–826. https://doi.org/10.1016/j.neuroimage.2005.10.014
Yang, L., Wilke, C., Brinkmann, B., Worrell, G.A., He, B., 2011. Dynamic imaging of ictal oscillations using non-invasive high-resolution EEG. NeuroImage 56, 1908–1917. https://doi.org/10.1016/j.neuroimage.2011.03.043
Yvert, B., Fischer, C., Bertrand, O., Pernier, J., 2005. Localization of human supratemporal auditory areas from intracerebral auditory evoked potentials using distributed source models. NeuroImage 28, 140–153. https://doi.org/10.1016/j.neuroimage.2005.05.056